Data-driven, projection-based respiratory motion compensation of PET data for cardiac PET/CT and PET/MR imaging

Martin Lyngby Lassen, PhD,[a,b] Thomas Beyer, PhD,[a] Alexander Berger, MSc,[a] Dietrich Beitzke, MD,[c] Sazan Rasul, MD, PhD,[d] Florian Büther, PhD,[e] Marcus Hacker, MD,[d] and Jacobo Cal-González, PhD[a]

[a] QIMP Team, Center for Medical Physics and Biomedical Engineering, Medical University of Vienna, Vienna, Austria
[b] Artificial Intelligence in Medicine program, Cedars-Sinai Medical Center, Los Angeles, California
[c] Division of Cardiovascular and Interventional Radiology, Department of Biomedical Engineering and Image-guided Therapy, Medical University of Vienna, Vienna, Austria
[d] Division of Nuclear Medicine, Department of Biomedical Engineering and Image-guided Therapy, Medical University of Vienna, Vienna, Austria
[e] Department of Nuclear Medicine, University Hospital Münster, Münster, Germany

Received May 31, 2018; accepted Jan 6, 2019
doi:10.1007/s12350-019-01613-2

Background. **Respiratory patient motion causes blurring of the PET images that may impact accurate quantification of perfusion and infarction extents in PET myocardial viability studies. In this study, we investigate the feasibility of correcting for respiratory motion directly in the PET-listmode data prior to image reconstruction using a data-driven, projection-based, respiratory motion compensation (*DPR-MoCo*) technique.**

Methods. **The *DPR-MoCo* method was validated using simulations of a XCAT phantom (Biograph mMR PET/MR) as well as experimental phantom acquisitions (Biograph mCT PET/CT). Seven patient studies following a dual-tracer (^{18}F-FDG/^{13}N-NH_3) imaging-protocol using a PET/MR-system were also evaluated. The performance of the *DPR-MoCo* method was compared against reconstructions of the acquired data (*No-MoCo*), a reference gate method (gated) and an image-based MoCo method using the standard reconstruction-transform-average (*RTA-MoCo*) approach. The target-to-background ratio (TBR_{LV}) in the myocardium and the noise in the liver (CoV_{liver}) were evaluated for all acquisitions. For all patients, the clinical effect of the *DPR-MoCo* was assessed based on the end-systolic (ESV), the end-diastolic volumes (EDV) and the left ventricular ejection fraction (EF) which were compared to functional values obtained from the cardiac MR.**

Results. **The *DPR-MoCo* and the *No-MoCo* images presented with similar noise-properties (CoV) ($P = .12$), while the *RTA-MoCo* and reference-gate images showed increased noise levels ($P = .05$). TBR_{LV} values increased for the motion limited reconstructions when compared to the *No-MoCo* reconstructions ($P > .05$). *DPR-MoCo* results showed higher correlation with the functional values obtained from the cardiac MR than the *No-MoCo* results, though non-significant ($P > .05$).**

Electronic supplementary material The online version of this article (https://doi.org/10.1007/s12350-019-01613-2) contains supplementary material, which is available to authorized users.

The authors of this article have provided a PowerPoint file, available for download at SpringerLink, which summarises the contents of the paper and is free for re-use at meetings and presentations. Search for the article DOI on SpringerLink.com.

Reprint requests: Martin Lyngby Lassen, PhD, Artificial Intelligence in Medicine program, Cedars-Sinai Medical Center, Los Angeles, California, USA; *MartinLyngby.Lassen@cshs.org*

1071-3581/$34.00

Conclusion. **The projection-based *DPR-MoCo* method helps to improve PET image quality of the myocardium without the need for external devices for motion tracking. (J Nucl Cardiol 2020;27:2216–30.)**

Key Words: Respiratory gating • listmode • motion correction • cardiac PET

Abbreviations	
CoV	Coefficient of variation
DDG	Data-driven gating
DPR-MoCo	Data-driven, projection based motion detection and compensation
LV	Left ventricle
MoCo	Motion compensation
MRI	Magnetic resonance imaging
MVS	Myocardial viability studies
RTA	Reconstruction transform average

See related editorial, pp. 2231–2233

INTRODUCTION

Myocardial viability studies are important tools in the evaluation of patients with ischemic heart disease.[1] These studies provide valuable information on the volume of both scar and hibernating tissues through evaluations of myocardial perfusion imaging and myocardial metabolism.[1] However, the quantitative accuracy of myocardial examinations is affected by image blurring from respiratory motion and cardiac contraction.

Gating techniques, which divide the cardiac contraction and/or respiration into several phases, have been suggested to limit cardiac motion effects. In cardiac PET, electrocardiogram (ECG) gating, using 3-lead ECG monitoring of the patient, has become the standard in clinical routine.[2] Traditionally, respiratory motion is detected using external markers, such as respiratory belts, infrared sensors or measurements of the nasal air temperature.[2,3] However, respiratory external markers frequently require time-consuming calibrations[4] and bear the risk of being inadequate throughout the acquisition due to changes in the respiratory baseline[5] or malfunctions during the acquisition.[6] Moreover, their use may be uncomfortable for patients. Therefore, there is a growing interest in obtaining the respiratory signal without the use of external devices and with as little patient instructions as possible. In this context, data-driven methods, which derive the respiratory signal directly from the acquired PET data (i.e., self-gating methods) or through the use of MR navigators in combined PET/MR systems, are promising alternatives to the use of external markers.[2,7–12]

However, gating approaches have the disadvantage of using only fractions of the acquired data, thus leading to increased noise levels in the resulting images.[13] This is particularly critical for myocardial PET-imaging, where corrections for both respiratory and cardiac motion are desired.[14] For this reason, motion compensation (MoCo) approaches have generated substantial interest. To date, two main approaches have been proposed: the reconstruct-transform-average (RTA) method, which relies on co-registrations of gated image-reconstructions,[15] and the motion-compensated image reconstruction, which is based on the inclusion of the motion information in the system matrix during the reconstruction.[16–18] Despite promising results,[19] these methods are not yet widely adopted in clinical routine due to complex setup procedures that involve user-defined reconstruction algorithms, which challenges a comparison to the results obtained in clinical settings.

Here, we propose a data-driven, projection-based respiratory MoCo (*DPR-MoCo*) approach for PET data acquired in PET-only, PET/CT or PET/MR systems. The proposed approach models the motion of each event in projection space and performs the correction event-by-event in the PET-listmode data, prior to the image reconstruction process.

MATERIALS AND METHODS

The proposed *DPR-MoCo* technique was implemented and validated through analytical simulations and phantom experiments and subsequently tested in clinical patients who underwent myocardial viability examinations.

Analytical Simulations

A 4D extended cardiac-torso (XCAT) phantom[20] was used for the analytical simulations based on the Siemens Biograph mMR PET/MR system. In contrast to an earlier approach by Tsoumpas and Cal-Gonzalez[21,22] the analytical simulation in our study generated a listmode file instead of gated sinograms (Supplementary File 1). Photon attenuation, random and scatter coincidences, as well as Poisson noise, were included in the simulations to mimic a realistic patient acquisition. Three different parametric models of cardio-respiratory motion were included in our simulations: (i) a 2 cm superior-inferior 1-dimensional respiratory motion (0.2 Hz); (ii) a 2 cm superior-inferior and 1 cm anterior-posterior respiratory motion (0.2 Hz); and (iii) the respiratory motion described in (ii) combined with a cardiac rate of 1 bps

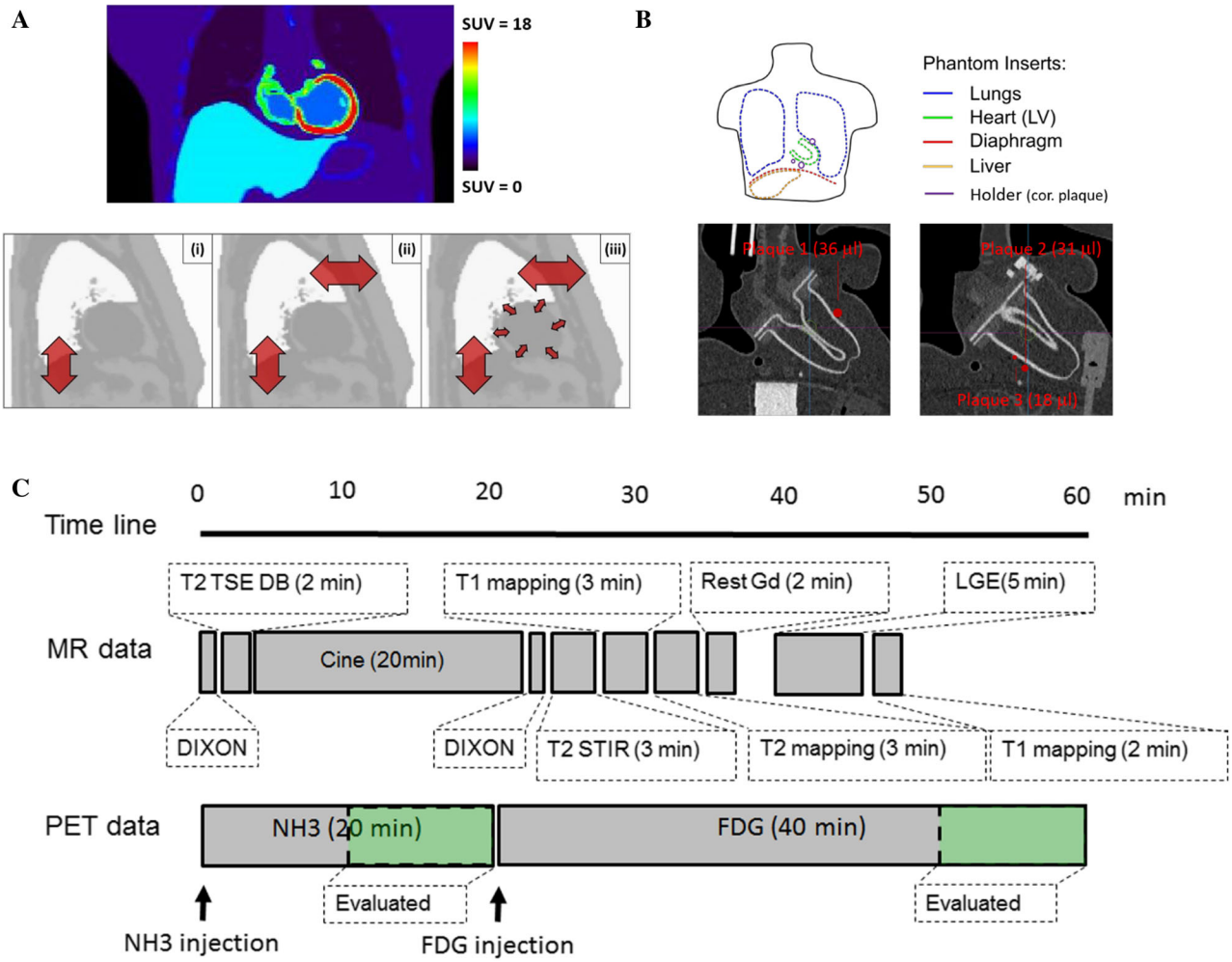

Figure 1. A Top—illustration of the simulated XCAT phantom (reference image used for the analytical simulations). Bottom—motion models included in the simulations: (i) 1D axial motion of 2 cm; (ii) 2D motion in the axial direction (2 cm) and in the anterior-posterior direction (1 cm); (iii) the respiratory motion described in (ii) combined with cardiac beating, 1 beat per second. Note that the cardiac motion in (iii) was simulated but not considered in the corrections. **B** Top—schematic design of the experimental phantom used for the validation of the data-driven respiratory motion detection. Bottom—CT image of the phantom illustrating the myocardial compartment and the three plaque-type lesions. **C** Flow-chart of dual-tracer PET/MRI protocol. Patients underwent simultaneous acquisitions of PET-based myocardial perfusion imaging employing ^{13}N-NH_3 and cine-acquisitions in the MR system. Myocardial viability was assessed through simultaneous acquisitions of PET employing ^{18}F-FDG and rest and late-gadolinium enhancement imaging protocols.

(Figure 1A). Note that the cardiac motion in (iii) was simulated, but not accounted for in the corrections. The following standardized uptake values (SUV) were used in both simulations: soft tissue = 2, liver = 7, myocardium = 18, lumen = 5, ribs = 3.

Five respiratory gates were created from the simulated listmode data. In the simulated dataset (iii), cardiac motion was included in the simulation but not considered in the corrections. The reconstruction of the simulated data was performed using the Software for Tomographic Image Reconstruction (STIR).[23]

Phantom Experiments

Two phantom studies were performed on a Siemens Biograph mCT PET/CT system at a collaborating site in Münster (Germany) (Figure 1B).[24] Three spherical plaque-type lesions of 36 mm, 31 mm and 18 mm^3 were attached to

Table 1. Patient demographics

Patient number	Age [years]	Gender	Injected activity [MBq]	
			^{13}N-NH$_3$	^{18}F-FDG
1	89	Male	578	318
2	73	Male	758	360
3	73	Female	743	323
4	72	Male	746	346
5	47	Male	450	287
6	66	Male	619	378
7	78	Female	643	292

the myocardium inside the phantom (Figure 1B). The studies were acquired either with or without phantom motion (No-Motion). The No-Motion acquisition was acquired for 10 minutes, while the study with motion effects was acquired over 30 minutes. The latter experiment simulated cardiac contractions every 1.9 seconds with a respiratory cycle of 4.6 seconds, as described by Cal-Gonzalez et al.[22] The myocardium-to-lumen ratio in the experimental phantom acquisition was 5-to-1. A respiratory signal obtained using a respiratory belt (Anzai AZ-733V) was used for validation of the data-driven respiratory detection.

Patient Studies

Seven patients (Table 1) undergoing myocardial viability examinations prior to revascularization procedures were enrolled and followed a combined PET/MR imaging protocol using a fully integrated PET/MR system (Siemens Biograph mMR, Siemens Healthineers, Erlangen, Germany).

All patients fasted for 4 hours prior to the ^{18}F-FDG examination in order to switch the patients to glucose metabolism. All patients were administered Acipimox (250 mg) to stimulate the uptake of the ^{18}F-FDG. Patients underwent dynamic acquisitions of myocardial perfusion imaging employing ^{13}N-NH$_3$ and metabolism studies employing ^{18}F-FDG in a combined PET/MR imaging protocol (Figure 1C). The study was approved by the institutional review board (IRB No.: 1832/2016).

The proposed motion compensation was evaluated on PET-emission data from the last 10 min of the acquisitions (^{13}N-NH$_3$: (10-20) min, ^{18}F-FDG: (30-40) minutes) to ensure a high tracer-uptake in the myocardium, as suggested in guidelines for myocardial metabolism imaging by the American Society of Nuclear Cardiology (ASNC).[25] All acquisitions were reconstructed using DIXON-attenuation correction maps in the clinical reconstruction tools (OSEM 3i21s, 4mm Gaussian filter).[26]

Data-Driven, Projection-Based Respiratory Motion Compensation (*DPR-MoCo*)

Standard clinical routine assessments involve image reconstruction of the acquired PET-data without any motion limiting post-processing (Figure 2A). The proposed *DPR-MoCo* technique involves two steps, (1) extraction of the respiratory signal and respiratory gating of the PET-images; (2) extraction of motion vector fields (MVF) and projection based respiratory MoCo.

In brief, in step (1) the respiratory signal was extracted from the PET-listmode file and used for an amplitude data-driven gating (DDG) of the obtained PET-list data (see subsection: *DDG*) (Figure 2B). In step (2), the MVFs were obtained from non-rigid, projection-based co-registrations of the myocardium for all respiratory gated images (Figure 3A) (see ''Extraction of the motion vector fields''). Following their extraction, the MVF's were used to correct all individual events in the acquired listmode data (Figure 3B), thus providing a data-driven, projection-based motion compensation (*DPR-MoCo*) (see ''Projection-based respiratory motion compensation'').

Respiratory motion detection (DDG)

To ensure accurate detection of the respiratory signal, we propose to extract the respiratory signals from the myocardium only. This was achieved by using a bounding-box that covered the myocardial outline plus 2.5 cm in each direction and forward projecting the bounding-box to projection space (sinogram space). In this study, we used a center-of-mass-based assessment of the count-rates obtained within the bounding box for 100 ms long time-intervals (Eq. 1).

$$\text{Center of mass } (t) = \frac{\sum_i i \cdot T(i,t)}{\sum_i T(i,t)} \quad (1)$$

where T is the histogram for the time segment t and i the slice number of the myocardial slice evaluated. The extracted respiratory signal was filtered using a moving

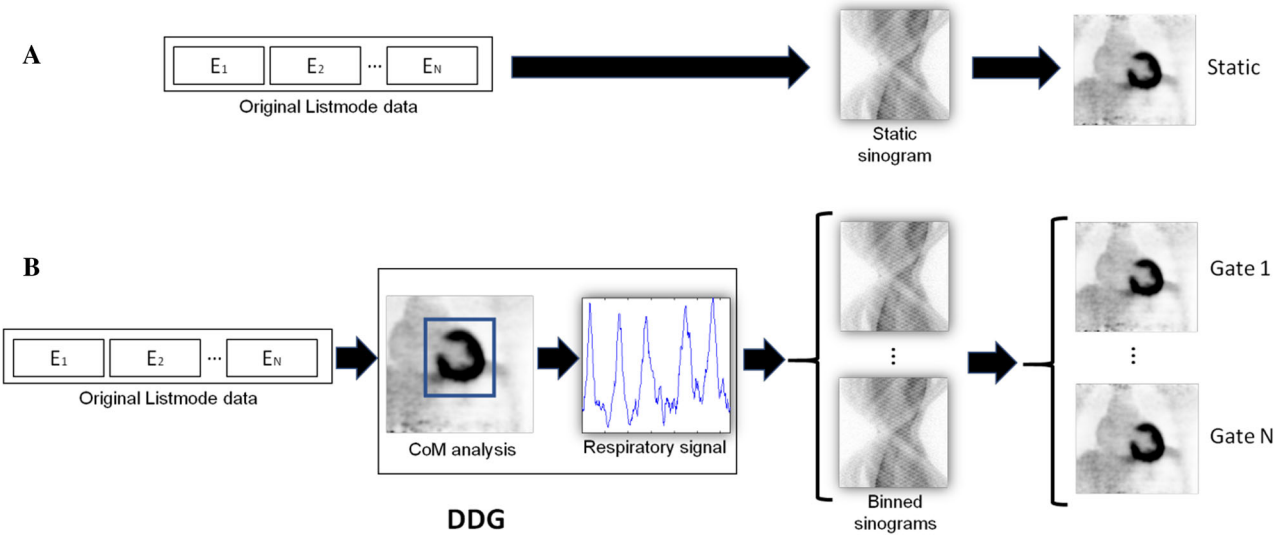

Figure 2. Data-driven motion detection. **A** Standard clinical reconstruction set-up employs the acquired listmode file with all stored events (E_1, E_2, …, E_N) during the acquisition. The resulting reconstruction has respiratory motion embedded in images, thus, degrading the image-quality. **B** The proposed DDG extracts the respiratory signal from the listmode file, followed by a respiratory gating of the acquired data.

average filter (0.3 seconds) to remove the 1Hz overlay signal introduced by the cardiac contractions (Figure 2B). Following filtering, the respiratory signal was used for an 4-bin amplitude-based gating (10-95-percentile of the respiratory range) of the PET listmode data and subsequent reconstruction in the vendor provided reconstruction toolbox (e7-tools, Siemens) [27] (Figure 2B).

Extraction of the motion vector fields

We propose to extract the MVF's using projections of the gated images, to limit the risk of artifacts in the motion compensation (Figure 3A). The MVFs were extracted using three steps: first the myocardium was segmented for all respiratory gated images, which improved the definition of the MVF by suppression of the activity in the sub-diaphragm regions[28] (Figure 3A). Then the segmented images were forward projected by using a Siddon's ray tracing algorithm, to obtain ideal, noise-free, gated projections from which the respiratory MVFs were calculated (Figure 3A). These ideal projections were obtained using the forward projector available in the STIR-toolbox.[23] Third, the sinogram-based MVFs were obtained from non-rigid co-registrations of the projected data using the Medical Imaging Registration Toolbox (MIRT)[29] (Figure 3A). All gates were co-registered to the end-expiratory breath-hold position using a sum-of-square difference assessment.

Projection-based respiratory motion compensation. The extracted respiratory MVFs were used to create a motion compensated listmode (LM) file (Figure 3B). Motion compensation was achieved by applying the defined MVF's to each event in the original listmode file. To ensure correct normalization of the data, the ratios of the normalization of the original and the motion-compensated positions were calculated and stored in an independent pseudo-LM file (Figure 3B). The respiratory MoCo sinograms were obtained from a combined binning of these two listmode files, followed by reconstruction using the vendor provided reconstruction tools.

Reconstruction Transformation Average (*RTA-MoCo*)

The *DPR-MoCo* method was validated against an image-based *RTA-MoCo*, in which the four amplitude-based reconstructions were co-registered to end-expiratory breath-hold position, as used for the *DPR-MoCo*.[15] The image-based MVFs used for the *RTA-MoCo* were obtained in the MIRT software using the same segmentations as employed for the *DPR-MoCo* method, thus ensuring comparable results.

Data Analysis

A total of four different image-reconstructions were evaluated for the simulations, the phantom study and the patient examinations: reconstructions of the acquired data without any motion compensation (*No-MoCo*), a reference gate (*Gated*), an RTA based reconstruction (*RTA-MoCo*) as well as the *DPR-rMoCo* images (Table 2). In case of the simulated data and phantom acquisitions, we also included the reference images without any motion (No-Motion). In addition, two ECG-gated reconstructions were performed for the patient datasets, using the acquired data (*No-MoCo-ECG*) and

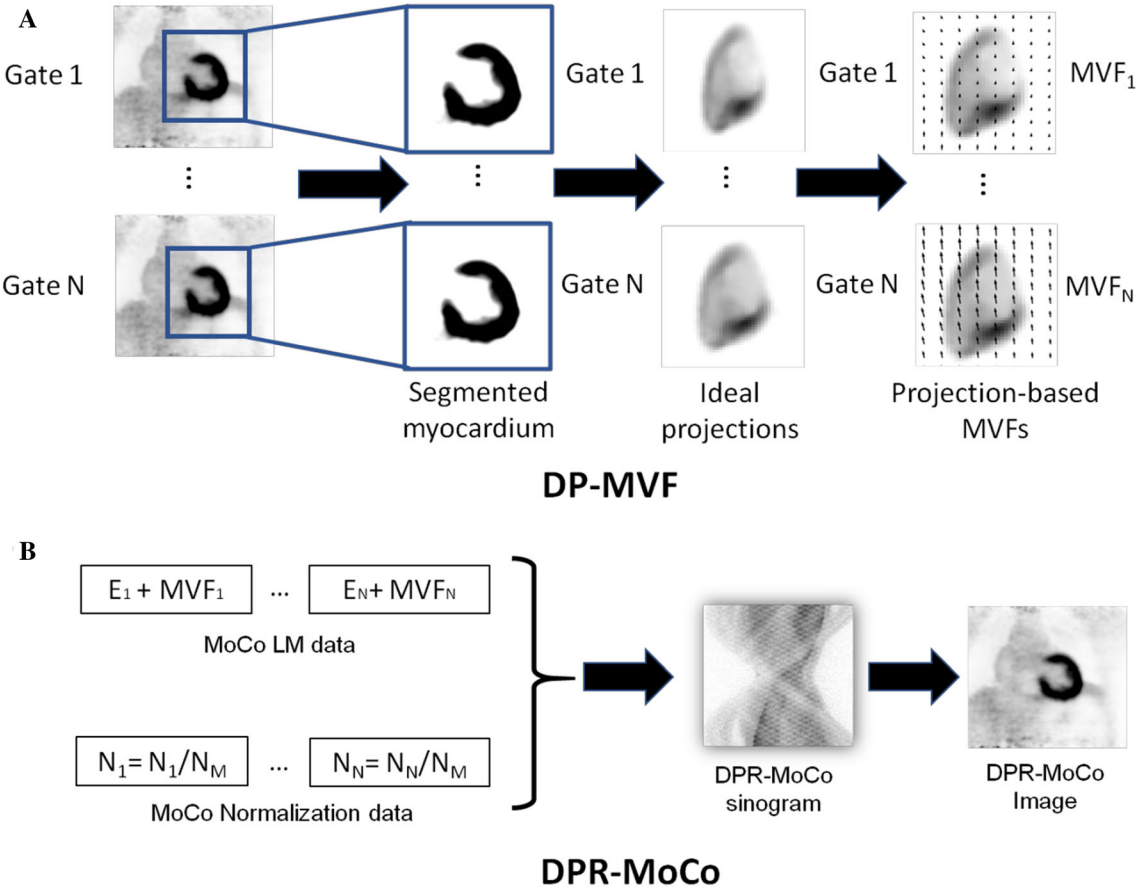

Figure 3. Definition of the projection-based motion vector fields (MVF) and the *DPR-MoCo* method. **A** Respiratory motion vector fields (MVF) are extracted from forward-projections of segmentations of the myocardium obtained for each respiratory phase (see Figure 2B). **B** The extracted MVFs are used to correct for the respiratory motion directly in the listmode file. An additional normalization listmode file is created to compensate for changes in the normalization when moving the individual prompts. A fully-respiratory motion compensated image is reconstructed using the vendor provided software.

the *DPR-rMoCo* (*DPR-ECG*). The ECG-gated datasets PET datasets were compared to the cardiac MR functional assessment of the myocardium using Medis MR Suite/Qmass toolbox (Medis, Leiden, the Netherlands).

A total of 10 figures-of-merit (FoM), consisting of both mathematical and clinical evaluations (Cedars-Sinai QPS/QGS 2013 version, Cedars-Sinai Medical Center, Ca, USA), were evaluated (Table 3). The mathematical FoM included: (1) the target-to-background ratios of the left ventricle (TBR_{LV}). Here the myocardium was segmented using a 41% SUV-max assessment, while the background was calculated from a spherical VOI (2.5 cm^3) inserted in the left atrium. (2) The noise in the images, which was assessed using the coefficient of variation (CoV_{liver}) in a 15 cm^3 spherical VOI inserted in the liver (3). The axial translations measured in the myocardium for the experimental phantom and patient acquisitions. The following FoM were used for the clinical evaluation: the lumen of left ventricle, the scar-size (^{18}F-FDG data), the total perfusion defect (TPD) (^{13}N-NH_3 data), end-systolic volume (ESV), end-diastolic volume (EDV), the stroke-volume (SV) and the ejection fraction (EF).

Statistical Analyses

The *Gated, RTA-MoCo and DPR-MoCo* images were compared to the *No-MoCo* reconstructions using one-way analyses of variance (1-way ANOVA) for all FoM's. The statistical analyses were corrected using a Dunnet correction to compensate for the multiple comparisons.[30]

RESULTS

Analytical Simulations

Figure 4 shows selected coronal views of the reconstructed images of the XCAT phantom with corresponding line profiles for different motion-patterns

Table 2. Motion detection and compensation techniques employed for the acquired PET-data (phantom acquisitions and patient examinations) and their respective characteristics

MoCo technique	Motion detection	MVF measurement	Motion compensation	MoCo+ECG gating
No-motion	No	N/A	No	No (ECG-gating only)
Gated (respiratory)	DDG	N/A	No	No
DPR-MoCo	DDG	Projection-based	Projection-based	Yes
RTA-MoCo	DDG	Image-based	Image-based	No

The two motion compensation techniques (Data-driven, projection-based respiratory motion compensation (*DPR-MoCo*) and reconstruction transform average (*RTA-MoCo*) employ different techniques for motion detection and compensation
DDG, data-driven gating

Table 3. Figures of merit (FoM) for the evaluation of the proposed *DPR-MoCo* method

	Simulations	Phantom data	Patient data
Mathematical figures-of-merit			
Respiratory translation	No	✔	✔
CoV_{Liver}	✔	✔	✔
TBR_{LV}	✔	✔	✔
Clinical figures of merit			
Lumen of left ventricle	No	No	✔
Scar size	No	No	✔
TPD	No	No	✔
ESV	No	No	✔
EDV	No	No	✔
SV	No	No	✔
EF	No	No	✔

The mathematical FoM included the respiratory translations (measured in the respiratory gated images), the Coefficient of Variation within the liver (CoV_{liver}) and the target-to-background ratios of the left ventricle (TBR_{LV}). Clinical FoM were obtained from Cedars QGS software (Cedars Sinai) and included the scar-size (^{18}F-FDG data), the total perfusion defect (TPD) (^{13}N-NH_3 data), end-systolic volume (ESV), end-diastolic volume (EDV), the stroke-volume (SV) and the ejection fraction (EF)

introduced in the simulations (1D, 2D). Upon visual inspection of the reconstructed images the *DPR-MoCo* and *RTA-MoCo* yield improved image-quality, with higher contrast and similar levels of noise. Upon quantitative evaluation, *DPR-MoCo* and *RTA-MoCo* images have TBR_{LV} and CoV_{liver} values comparable to the *No-Motion* images (Table 4). The *No-MoCo* images had lower TBR_{LV} values, while the single-gate reconstructions presented much higher CoV_{liver} values (Table 4).

Phantom Experiments

A high correlation (99% detection rate) was observed for the respiratory signal obtained using the proposed DDG and external markers (Figure 5). Both signals provided a strong respiratory peak in the Fourier spectrum for a frequency of 0.216 Hz, which corresponds to a respiratory signal with period of 4.6 seconds. The corresponding MVFs obtained for the segmented myocardium recovered 75% of the motion exerted to the myocardium in the axial direction (Table 4). Comparable noise levels were observed for the *No-MoCo, RTA-MoCo* and *DPR-MoCo* images (Table 4). Improved TBR_{LV} were seen in the *DPR-MoCo* and *RTA-MoCo* images, when compared to the *No-MoCo* reconstructions (Figure 5). The TBR_{LV} values for the *DPR-MoCo* and *RTA-MoCo* images were, however, not recovering the values obtained for the *No-Motion* images of the static phantom.

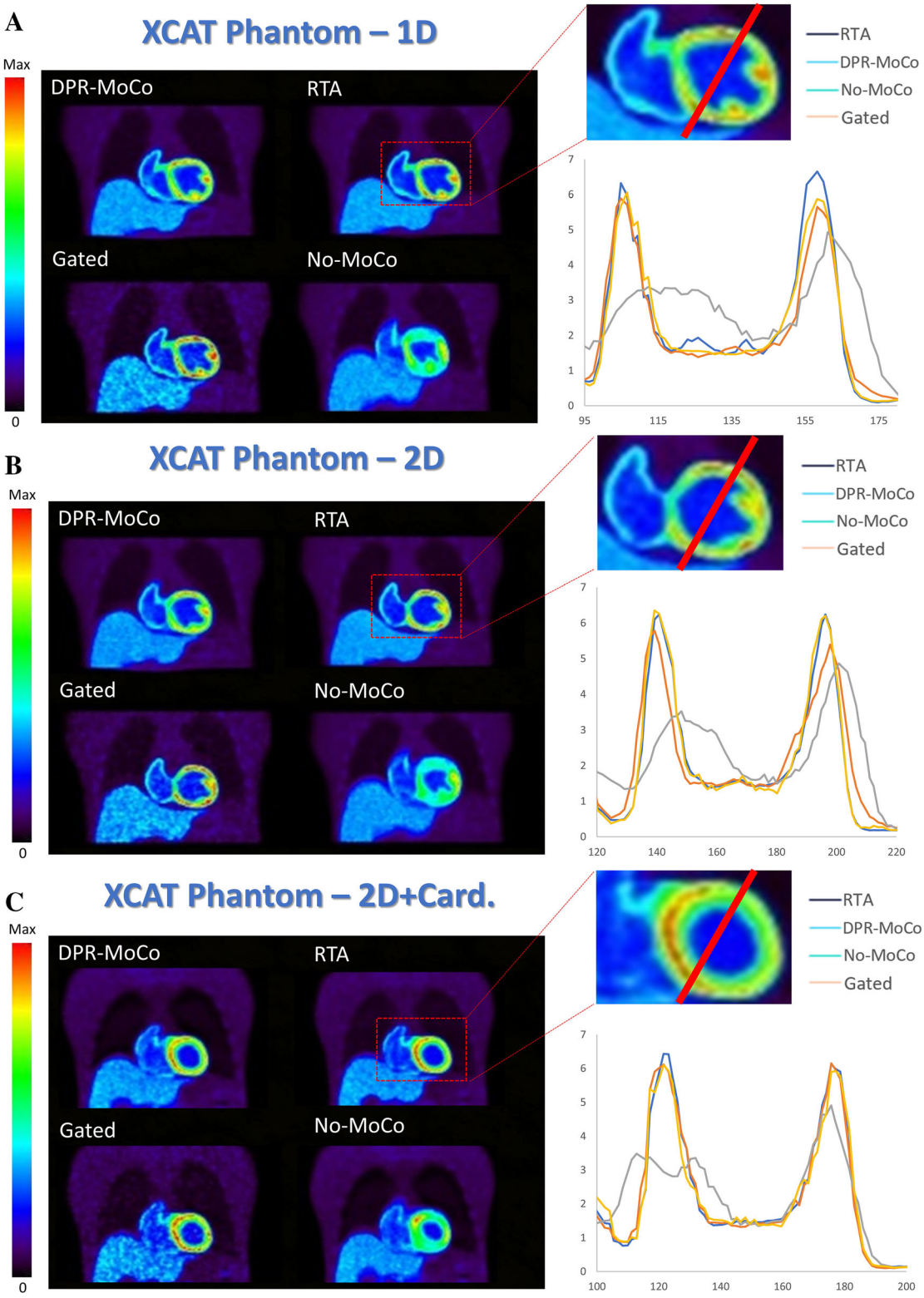
A
XCAT Phantom – 1D
Max
0
DPR-MoCo
RTA
Gated
No-MoCo
RTA
DPR-MoCo
No-MoCo
Gated
0 1 2 3 4 5 6 7
95 115 135 155 175
B
XCAT Phantom – 2D
Max
0
DPR-MoCo
RTA
Gated
No-MoCo
RTA
DPR-MoCo
No-MoCo
Gated
0 1 2 3 4 5 6 7
120 140 160 180 200 220
C
XCAT Phantom – 2D+Card.
Max
0
DPR-MoCo
RTA
Gated
No-MoCo
RTA
DPR-MoCo
No-MoCo
Gated
0 1 2 3 4 5 6 7
100 120 140 160 180 200

◀**Figure 4.** Simulated XCAT phantom. **A** Comparison of *DPR-MoCo*, *RTA-MoCo*, Gated and *No-MoCo* images for the simulations with 1D axial respiratory motion model. **B** Same images, but with a 2D axial + anterior/posterior motion model. The corresponding line profiles through the myocardium are depicted in the right side of the figure. A significant improvement in image contrast, while preserving noise properties, can be observed for the *DPR-MoCo* and the *RTA-MoCo* images. **C** Same images, but with a 2D axial + anterior/posterior + cardiac motion model. Note, the cardiac motion in (iii) was simulated but not accounted for in the corrections.

Patient Studies

***DPR-MoCo*: static myocardial examination.** Significant respiratory motion was observed for the patient acquisitions, with translations of up to 31 mm in the axial direction (Table 5). Improved resolution recoveries were observed when applying motion limiting (Gated) or motion compensation (*DPR-MoCo*, *RTA-MoCo*) techniques (Figure 6, Table 6), resulting in contour sharpening of TPD and better scar delineations on the polar-maps. Assessments of the image-quality reveal statistically significantly increased noise-levels for the *Gated* and *RTA-MoCo* images, while the *DPR-MoCo* have slightly better image-quality across the patients, although the differences were not statistically significant (Table 6). The individual assessment of CoV_{Liver}, left ventricular volume and CBR_{LV} for the different image reconstruction methods are provided in the supplementary data (Figure SM1). The reconstructed images for two patients are also provided in the supplementary data (Figures SM2 and SM4).

***DPR-MoCo* + ECG-gating.** Diastolic and systolic phases of the *DPR-MoCo* and standard LM-based reconstructions showed marked differences when the polar maps were analyzed using the clinical evaluation software (Figure 7, Supplementary Figures 3, 5). The patient displayed in Figure 7 had confirmed 3-vessel disease as visualized by a general reduced radio-tracer uptake (^{13}N-NH_3 and ^{18}F-FDG) in the myocardial PET images and the corresponding polar maps. A slight increase in the tracer-uptake is seen for the anterior part of the myocardium when applying the *DPR-MoCo*.

Grouped analyses of the ESV, EDV, SV and EF revealed improved delineations of the left-ventricular wall after motion compensation across the patients, shown as reduced ESV and EDV values. Furthermore, the *DPR-MoCo* images revealed higher correlation with the cardiac MRI extracted EF values (Table 7).

DISCUSSION

In this study, we describe the feasibility of a data-driven, projection-based motion detection and correction method (*DPR-MoCo*) for cardiac PET imaging. The *DPR-MoCo* method was evaluated in simulations, phantom studies and clinical patients. In all cases, we observed a clear improvement in the reconstructed PET images when employing the proposed *DPR-MoCo*, with increased TBR_{LV} values and similar noise levels to the ones obtained in *No-MoCo* images (Table 4).

Table 4. CoV_{liver} and the TBR_{LV} values obtained from images reconstructed with *DPR-MoCo* compared with the values obtained from images reconstructed without MoCo (*No-MoCo*), gated images (*Gated*), *RTA-MoCo* and acquisitions without motion (*No-Motion*)

	No-MoCo	Gated	*DPR-MoCo*	*RTA-MoCo*	No-motion
CoV_{Liver} (%)					
Simulation (1D)	3.0	6.1	2.6	2.2	3.0
Simulation (2D)	3.0	6.2	2.5	2.4	3.0
Simulation (2D + cardiac)	3.6	5.4	2.4	2.3	3.0
Phantom experiment	10.1	17.4	11.1	11.9	11.2
TBR_{LV}					
Simulation (1D)	1.8	3.0	2.9	2.9	3.0
Simulation (2D)	1.8	2.9	2.8	2.9	3.0
Simulation (2D + cardiac)	1.5	2.3	2.2	2.2	3.0
Phantom experiment	7.4	7.7	8.1	7.8	12.8
	Measured axial motion (mm)			**Simulated axial motion (mm)**	
Phantom experiment	15.5			20.0	

Table 5. Respiratory translations (mm) observed for the respiratory gated images

Patient	^{13}N-NH$_3$				^{18}F-FDG			
	Axial		Transaxial		Axial		Transaxial	
	Mean	Max	Mean	Max	Mean	Max	Mean	Max
1	10.6	31.3	3.5	15.0	3.3	11.1	1.3	5.9
2	3.3	13.9	3.6	15.8	3.8	15.6	2.7	10.5
3	3.5	27.0	3.3	19.8	4.5	25.7	2.8	11.2
4	6.9	28.0	7.3	28.9	3.2	14.3	3.8	20.9
5	2.0	10.4	1.9	6.5	2.4	13.2	2.4	9.4
6	7.4	27.3	3.8	17.7	6.1	24.8	3.1	18.5
7	8.8	24.5	3.6	15.8	7.0	23.5	3.0	13.7
Mean±SD	6±3	23±8	4±2	17±7	4±2	18±6	3±1	13±5

The maximum translation is calculated as the maximum displacement between the template gate and the reference gate for an individual patient

Table 6. Mathematical FoM obtained for the patient analyses averaged across all seven patients

	^{13}N-NH$_3$				^{18}F-FDG			
	Wall Volume	**TBR$_{LV}$**	**CoV Liver**	**TPD**	**Wall Volume**	**TBR$_{LV}$**	**CoV Liver**	**Scar**
No-MoCo	161	45	0.08	23	150	39.1	0.08	23
Gated	**158**	48	**0.11**	25	**146**	35	**0.13**	25
DPR-MoCo	160	48	0.08	24	150	41	0.08	24
RTA-MoCo	160	47	**0.09**	24	148	43	**0.11**	24

FoM values in bold are statistically significant different to the *No-MoCo* corresponding FoM value ($P \leq 0.05$). Increased TBR$_{LV}$ and total perfusion defect (TPD) were reported for the *Gated, DPR-MoCo* and *RTA-MoCo* images. The *No-MoCo* and *DPR-MoCo* images had reduced noise (CoV Liver), when compared to the *Gated* and *RTA-MoCo* images. FoM = Figures of Merit

Furthermore, relative changes between *No-MoCo* and *DPR-MoCo* reconstructions were reported for several parameters of clinical interest, such as the ESV, the EDV, and the EF.

The performance of the *DPR-MoCo* was evaluated by means of analytical simulations of the XCAT phantom. We demonstrated a good performance of the proposed *DPR-MoCo* (Figure 4 and Table 4). A high number of acquired counts was simulated (500 million counts per gated sinogram), leading to reconstructed images with very low levels of noise (Table 4).

The proposed method (*DPR-MoCo*) was validated also in phantom studies by comparing the data-driven extracted respiratory signals to the respiratory signals obtained from using a respiratory belt (Anzai AZ-733V) (Figure 5). Here, nearly perfect correlations between the respiratory signals were observed for the DDG technique, which translated into improvements of reconstructed images employing either gating or MoCo (Figure 5, Table 4). As expected, image noise levels did increase for the single-gate reconstructions when compared to image reconstructions using the full-acquired data: *No-MoCo*, *DPR-MoCo and RTA-MoCo* (Tables 4 and 6).

Further, the clinical effect of the *DPR-MoCo* was assessed also in seven patients. We observed relative improvements in the visual quality of the reconstructed images after applying the *DPR-MoCo* (Figure 6, Table 6). However, these improvements were lower than expected and not statistically significant (Table 6).

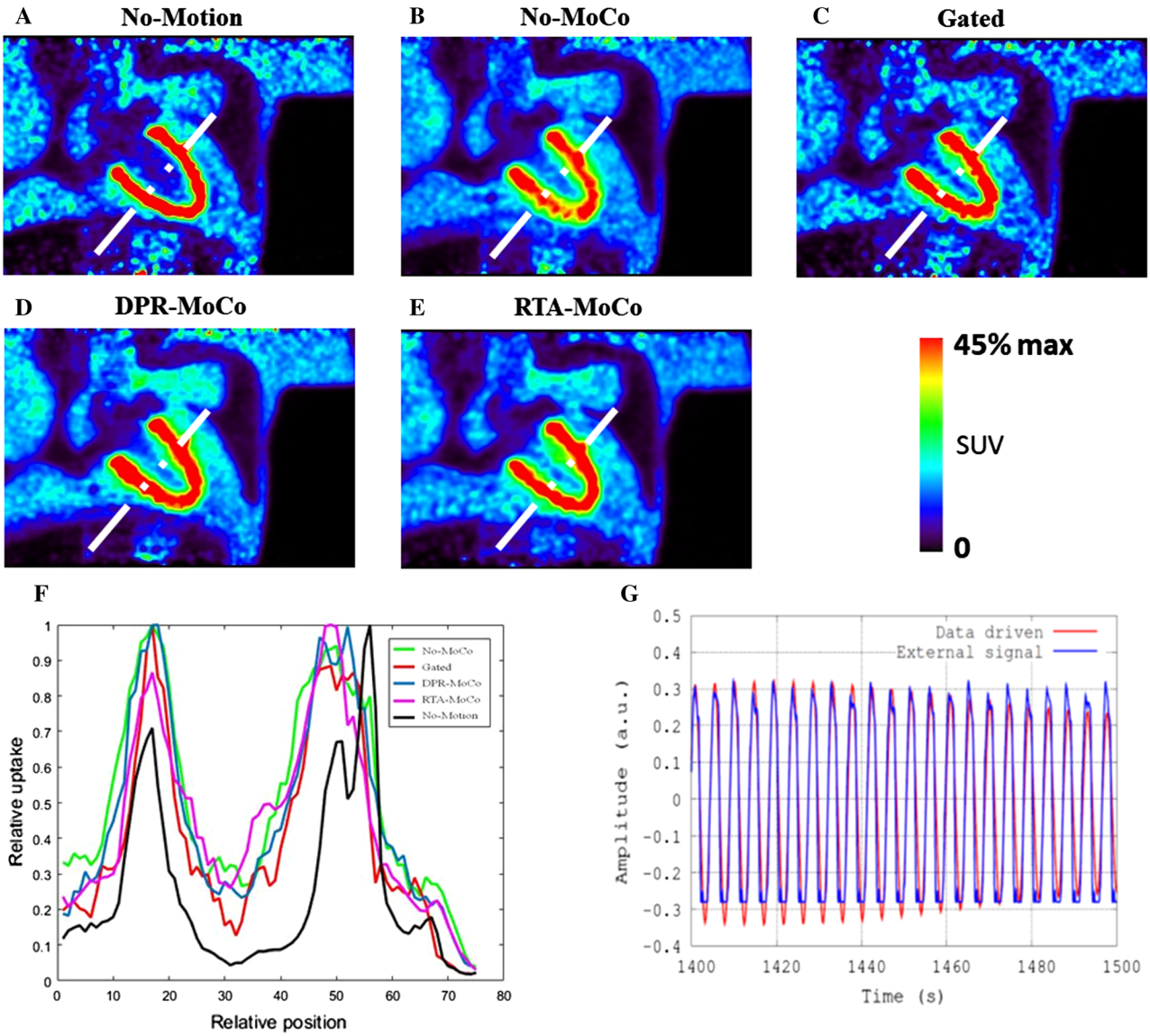

Figure 5. Experimental phantom study. **A** No-Motion, **B** *No-MoCo*, **C** Gated, **D** *DPR-MoCo* and **E** *RTA-MoCo*. One of the inserted plaque-type lesions is clearly visible in the images shown in panels A, C, D and E. **F** Line profile through the myocardium shows resolution recovery for the motion limited data when compared to the static images. **G** Respiratory signal obtained using the DDG (red) and external markers (blue), which shows an excellent overlap between them.

Nevertheless, we observed a higher impact of our proposed *DPR-MoCo* approach on the ^{13}N-NH_3 scans, due to increased respiratory translations introduced by the simultaneous acquisition of MR-cine sequences that require multiple breath-holds (Figure 1, Table 5).[31]

An important benefit of the proposed *DPR-MoCo* technique is the ability of performing ECG-gating of the listmode data including correction for respiratory motion. Evaluations of the ECG-gated PET-images employing the *DPR-MoCo* and *No-MoCo* datasets provided notably more consistent EF measures when compared to the cardiac MR measures following *DPR-MoCo*. The mitigated difference between the cMR and *DPR-MoCo* was introduced by enhanced delineations of the myocardial wall (Figure 7, Supplementary Figures 1-5) owing to the correction of the respiratory blur in the PET images. The relative improvement in the image-quality was correlated with the motion observed for the myocardium across patients. In cases with significant respiratory motion, such as the ^{13}N-NH3 studies (introduced by multiple breath-holds, required

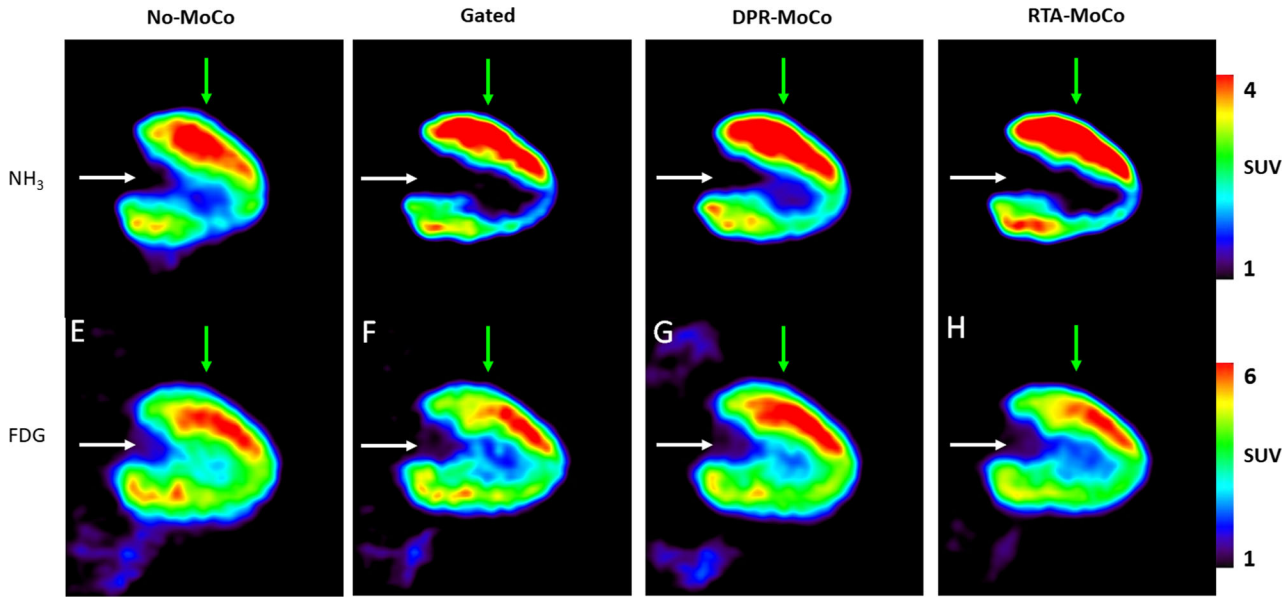

Figure 6. Comparison of image-quality obtained for the ^{13}N-NH_3 (top) and ^{18}F-FDG (bottom) scans for a patient #7. (A) *No-MoCo*, (B) Gated, (C) *DPR-MoCo* and (D) *RTA-MoCo* images are shown. Improved contrast recovery is seen for the Gated, *DPR-MoCo* and *RTA-MoCo* images, as improved delineation of the left-ventricular lumen (white arrow) and sharpening of the myocardial wall (green arrow).

by the cMR), we obtained higher image quality improvement after applying the MoCo techniques.

The proposed method has certain advances in terms of translation into clinical practice, as the method can be fully automatized. The current implementation offers a semiautomatic approach, which only requires manual entries in terms of segmentation of the myocardium. Automatic delineations of the myocardium can further improve the proposed technique to become fully automated, which currently is work in progress.

Despite being tested in a clinical setting with high count statistics, it is believed that this technique also works for other studies with low-count statistics such as coronary PET-studies for two reasons.[32] First, the DDG requires high contrast between the myocardium and the lungs, a requirement that is fulfilled for most tracers following the first-pass phase. The second reason is that the MVFs are extracted using ideal sinograms, obtained from projections of the respiratory gated images. These ideal projections contain is stable in terms of noise and are, thus, not affected by even low count statistics as can be expected in some applications.

Limitations of the *DPR-MoCo* Method

The sinogram-based definition of the MVFs is inherent to the proposed *DPR-MoCo* approach and can be argued as its major limitation since motion in image space is only partly reflected as motion in sinogram space. In this work, we assumed that the respiratory motion in the heart can be approximated by a simple motion pattern in 2D (axial and anterior-posterior), and therefore, the loss of information due to moving from image-to-sinogram space does not yield significant degradation of the accuracy of the motion model. However, for more complex motion patterns, e.g., cardio-respiratory motion, the proposed method will be challenged. Further investigations of the range of applicability of the *DPR MoCo* approach are required to understand its pitfalls.

Another limitation is the use of only four bins in the amplitude-based respiratory gating, which is known to possess a significant amount of intra-frame motion.[27] The effect of the *DPR-MoCo* is expected to be improved if using a higher number of respiratory bins, however, the increase in noise in the gated reconstructions may also reduce the accuracy of the resulting *DPR-MoCo* images. Further studies are required to find the optimal settings of this technique.

Finally, in view of the small size of the analyzed patient-cohort, a follow-up study related to the clinical evaluation of the proposed method based on a larger patient cohort has been initiated as well.

Table 7. Functional values obtained for the ECG-gated reconstructions of the *No-MoCo* and *DPR-MoCo* image reconstructions as well as the cardiac MR functional parameters, averaged across patients

	^{13}N-NH$_3$				^{18}F-FDG			
	ESV	**EDV**	**SV**	**EF**	**ESV**	**EDV**	**SV**	**EF**
No-MoCo	50	105	55	59	53	97	45	52
DPR-MoCo	47	99	53	58	48	91	43	54
cMR	55	107	52	55	55	107	52	55

Generally better comparison for EF were observed for the *DPR-MoCo* results, though not statistically significant
ESV, end systolic volume, *EDV*, end diastolic volume, *SV*, stroke volume and *EF*, ejection fraction, *cMR*, cardiac MRI

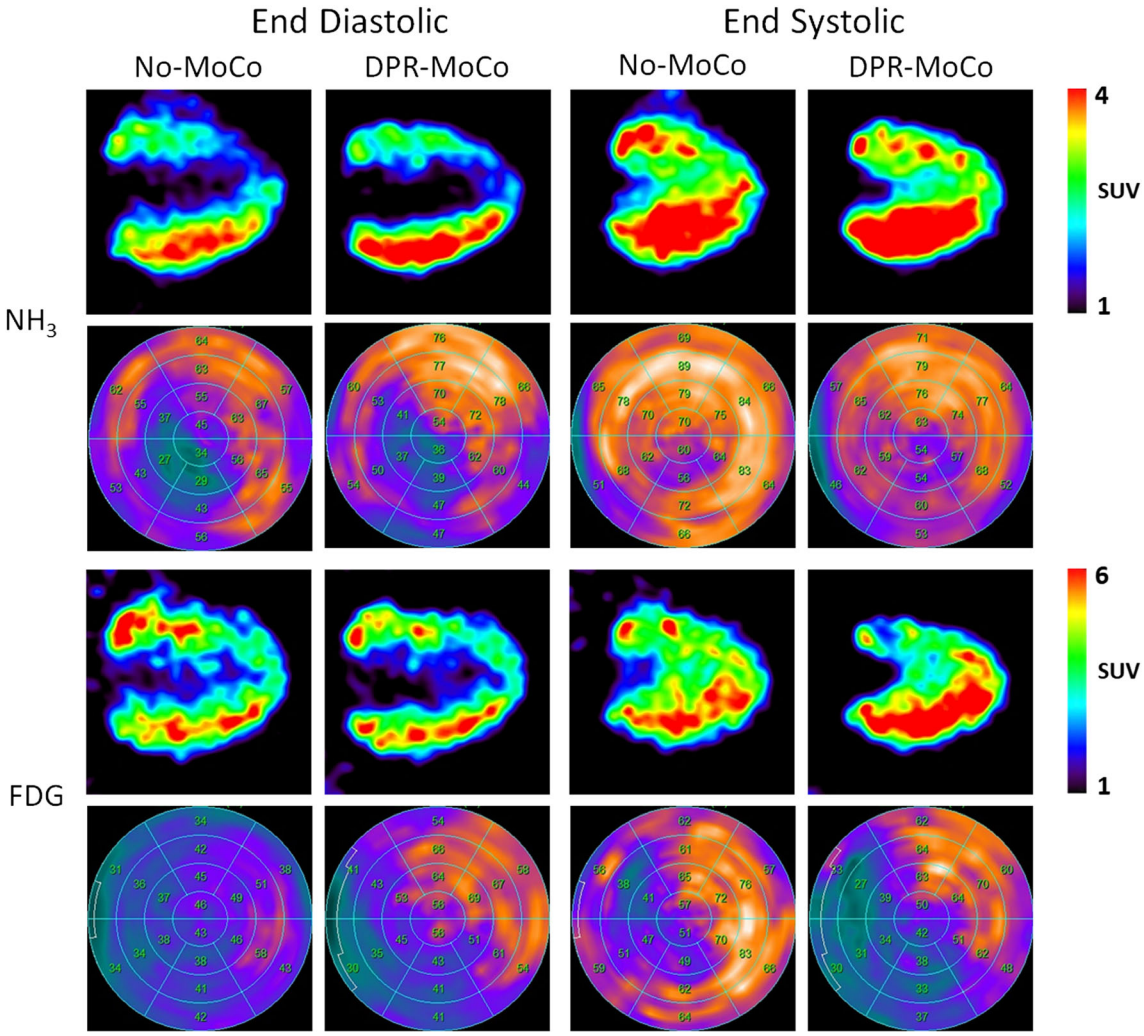

Figure 7. Comparison of End-Diastolic and End-Systolic images obtained for patient #7, Top: images and polar maps from the last 10 minutes of the ^{13}N-NH$_3$ scan. Bottom: images and polar maps from the last 10 min of the ^{18}F-FDG scan. *No-MoCo* ECG reconstructions are shown on the left while *DPR-MoCo* ECG-reconstructions are shown on the right.

NEW KNOWLEDGE GAINED

In this study, we demonstrated that a projection-based motion modeling and compensation technique can provide an image-quality of the heart comparable to already established methods.

CONCLUSION

This study proposes a data-driven MoCo technique for PET imaging. The proposed *DPR-MoCo* method applied to respiration and yields significant improvements in the image quality and quantification of the myocardial wall for ECG-gated reconstructions. To date, the methods have been validated for simple motion models and well-defined sources of tracer distribution in cardiac PET imaging.

Acknowledgments

We thank Piotr Slomka (Cedars-Sinai Medical Center) and Amir Fatemi (Medical University of Vienna) for helpful discussions. We also thank Klaus Schaefers for providing us with the experimental phantom data and for helpful discussions.

Disclosures

MH, TB and FB all have grants with Siemens Healthineers. None of the disclosures influenced the current study. In addition, TB has received royalties from Henry Stewart Lectutes. This disclosure did not influence the current study. MH also has given lectures sponsored by GE Healthcare, Bayer Healthcare and Siemens Healthineers. Furthermore MH, hold grants from Eli Lilly, Roche, BMS, Ipsen, ITM and EZAG. None of these disclosures influenced this study. MLL, AB, DB, SR, JCG has no conflict of interest or any disclosures relevant to this paper.

References

1. Galazka P, Di Carli MF. Cardiac PET/CT and prognosis. Cardiovasc Innov Appl 2016;2:47-59.
2. Büther F, Dawood M, Stegger L, et al. List mode-driven cardiac and respiratory gating in PET. J Nucl Med 2009;50:674-81. https://doi.org/10.2967/jnumed.108.059204.
3. Dawood M, Büther F, Stegger L, et al. Optimal number of respiratory gates in positron emission tomography: A cardiac patient study. Med Phys 2009;36:1775-84. https://doi.org/10.1118/1.3112422.
4. Giraud P, Houle A. Respiratory gating for radiotherapy: main technical aspects and clinical benefits. *ISRN Pulmonol*. 2013.
5. Lassen ML, Rasmussen T, Christensen TE, Kjær A, Hasbak P. Respiratory gating in cardiac PET: Effects of adenosine and dipyridamole. J Nucl Cardiol 2016. https://doi.org/10.1007/s12350-016-0631-z.
6. Liu C, Pierce LA II, Alessio AM, Kinahan PE. The impact of respiratory motion on tumor quantification and delineation in static PET/CT imaging. Phys Med Biol 2009;54:7345.
7. Kesner AL, Bundschuh RA, Detorie NC, et al. Respiratory gated PET derived in a fully automated manner from raw PET data. IEEE Trans Nucl Sci 2009;56:677-86. https://doi.org/10.1109/TNS.2009.2016341.
8. Grimm R, Fürst S, Souvatzoglou M, et al. Self-gated MRI motion modeling for respiratory motion compensation in integrated PET/MRI. Med Image Anal 2014;19:110-20. https://doi.org/10.1016/j.media.2014.08.003.
9. Munoz C, Kolbitsch C, Reader AJ, Marsden P, Schaeffter T, Prieto C. MR-based cardiac and respiratory motion-compensation techniques for PET-MR imaging. PET Clin 2016;11:179-91. https://doi.org/10.1016/j.cpet.2015.09.004.
10. Kesner AL, Kuntner C. A new fast and fully automated software based algorithm for extracting respiratory signal from raw PET data and its comparison to other methods. Med Phys 2010;37:5550-9. https://doi.org/10.1118/1.3483784.
11. Feng T, Wang J, Tang J, Wang X, Gao X. Impact of motion compensation and partial volume correction for 18F-NaF PET/CT imaging of coronary plaque. Phys Med Biol 2018;63:015005.
12. Munoz C, Kunze KP, Neji R, et al. Motion-corrected whole-heart PET-MR for the simultaneous visualisation of coronary artery integrity and myocardial viability: An initial clinical validation. Eur J Nucl Mol Imaging 2018. https://doi.org/10.1007/s00259-018-4047-7.
13. Nehmeh SA. Respiratory motion correction strategies in thoracic PET-CT imaging. PET Clin 2013;8:29-36. https://doi.org/10.1016/j.cpet.2012.10.004.
14. Slomka PJ, Rubeaux M, Le Meunier L, et al. Dual-gated motion-frozen cardiac PET with flurpiridaz F18. J Nucl Med 2015;56:1876-81. https://doi.org/10.2967/jnumed.115.164285.
15. Picard Y, Thompson CJ. Motion correction of PET images using multiple acquisition frames. IEEE Trans Med Imaging 1997;16:137-44. https://doi.org/10.1109/42.563659.
16. Manber R, Thielemans K, Hutton BF, et al. Practical PET respiratory motion correction in clinical PET/MR. J Nucl Med 2015;56:890-6.
17. Rahmim A, Qi J, Sossi V. Resolution modeling in PET imaging: Theory, practice, benefits, and pitfalls. Med Phys 2013;40:064301. https://doi.org/10.1118/1.4800806.
18. Tsoumpas C, Polycarpou I, Thielemans K, et al. The effect of regularization in motion compensated PET image reconstruction: A realistic numerical 4D simulation study. Phys Med Biol 2013;58:1759-73. https://doi.org/10.1088/0031-9155/58/6/1759.
19. Kolbitsch C, Ahlman MA, Davies-Venn C, et al. Cardiac and respiratory motion correction for simultaneous cardiac PET/MR. J Nucl Med 2017;58:846-52.
20. Segars WP, Sturgeon G, Mendonca S, Grimes J, Tsui BMW. 4D XCAT phantom for multimodality imaging research. Med Phys 2010;37:4902-15. https://doi.org/10.1118/1.3480985.
21. Tsoumpas C, Buerger C, Mollet P, Marsden PK. Fast analytic simulation toolkit for generation of 4D PET-MR data from real dynamic MR acquisitions. J Phys 2011;317:12020.
22. Cal-González J, Tsoumpas C, Lassen ML, et al. Impact of motion compensation and partial volume correction for 18F-NaF PET/CT imaging of coronary plaque. Phys Med Biol 2017;63:15005.
23. Thielemans K, Tsoumpas C, Mustafovic S, et al. STIR: Software for tomographic image reconstruction release 2. Phys Med Biol 2012;57:867.
24. Fieseler M, Kugel H, Gigengack F, et al. A dynamic thorax phantom for the assessment of cardiac and respiratory motion correction in PET/MRI: A preliminary evaluation. Nucl

Instruments Methods Phys Res Sect A Accel Spectrom, Detect Assoc Equip 2013;702:59-63. https://doi.org/10.1016/j.nima.2012.09.039.

25. Dilsizian V, Bacharach SL, Beanlands RS, et al. ASNC imaging guidelines/SNMMI procedure standard for positron emission tomography (PET). Nucl Cardiol Proc 2016. https://doi.org/10.1007/s12350-016-0522-3.
26. Martinez-Möller A, Souvatzoglou M, Delso G, et al. Tissue classification as a potential approach for attenuation correction in whole-body PET/MRI: Evaluation with PET/CT data. J Nucl Med 2009;50:520-6.
27. Dawood M, Buther F, Lang N, Schober O, Schafers KP. Respiratory gating in positron emission tomography: A quantitative comparison of different gating schemes. Med Phys 2007;34:3067-76. https://doi.org/10.1118/1.2748104.
28. Di Carli MF, Dorbala S, Meserve J, El Fakhri G, Sitek A, Moore SC. Clinical myocardial perfusion PET/CT. J Nucl Med 2007;48:783-93. https://doi.org/10.2967/jnumed.106.032789.
29. Myronenko A, Song X. Intensity-based image registration by minimizing residual complexity. IEEE Trans Med Imaging 2010;29:1882-91. https://doi.org/10.1109/TMI.2010.2053043.
30. Dunnett CW. A multiple comparison procedure for comparing several treatments with a control. J Am Stat Assoc 1955;50:1096-121.
31. Carr JC, Simonetti O, Bundy J, Li D, Pereles S, Finn JP. Cine MR angiography of the heart with segmented true fast imaging with steady-state precession. Radiology 2001;219:828-34.
32. Joshi NV, Vesey AT, Williams MC, et al. 18F-fluoride positron emission tomography for identification of ruptured and high-risk coronary atherosclerotic plaques: A prospective clinical trial. Lancet 2014;383:705-13. https://doi.org/10.1016/S0140-6736(13)61754-7.